# Semiconductor device simulation using generalized mobility models

by Steven E. Laux Robert G. Byrnes

A method for discretizing the semiconductor transport equations using generalized mobility models is developed as an extension of the Scharfetter-Gummel finite difference approach. The method is sufficiently general to be applicable to nearly arbitrary empirical mobility models (including those for MOS surface effects) and may be used on a variety of mesh types in two or three dimensions. The impact of generalized mobility models on the sparsity of our resulting discrete equations is discussed. Convergence rate of a Newton's method linearization of the nonlinear system of equations is measured and interpreted. Some computational results from a study of shortchannel MOSFETs are presented to illustrate the approach.

### 1. Introduction

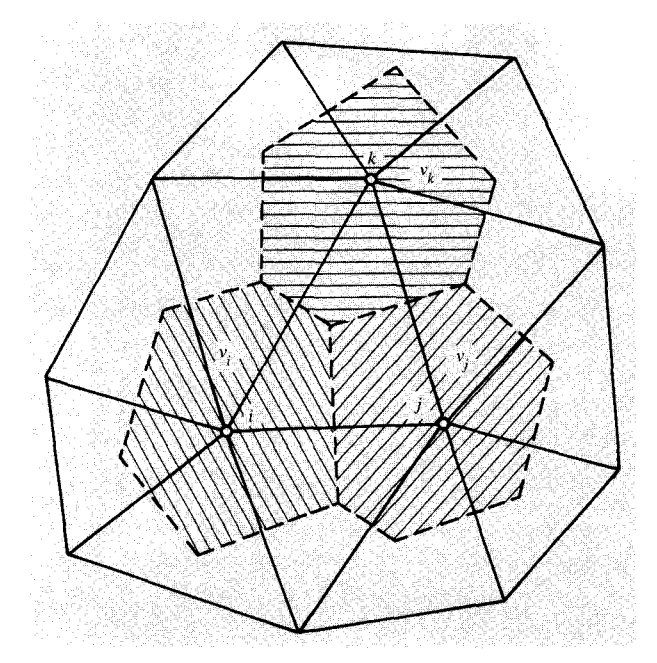
Many physical models have been proposed for the simulation of different classes of semiconductor devices, and a correspondingly wide range of numerical algorithms have been developed to obtain solutions for practical device analysis [1–5]. The approach which is the most successful, however, in terms of generality and practicality, and is certainly the most widely used, is the macroscopic model

**°Copyright** 1985 by International Business Machines Corporation. Copying in printed form for private use is permitted without payment of royalty provided that (1) each reproduction is done without alteration and (2) the *Journal* reference and IBM copyright notice are included on the first page. The title and abstract, but no other portions, of this paper may be copied or distributed royalty free without further permission by computer-based and other information-service systems. Permission to *republish* any other portion of this paper must be obtained from the Editor.

involving the semiconductor transport equations [6]. The model describes electrostatic fields in terms of the Poisson equation, charge conservation in terms of continuity equations, and transport properties due to drift and diffusion in terms of hole and electron current transport equations.

Analysis of the behavior of small (submicron geometry) devices for VLSI has revealed the necessity of incorporating into the model descriptions of nonlinear transport properties due to special scattering processes, carrier heating, quantization effects, etc. These physical phenomena probably represent the limits of validity of the macroscopic model itself, and the model may eventually have to be replaced with a microscopic quantum transport theory. However, until the conduction mechanisms are better understood and faster solution algorithms are developed, the most practical approach is to improve the macroscopic model by introducing nonlinear, empirical mobility relations into the current transport equations. The earliest mobility models attempted to account for bulk effects, such as velocity saturation and impurity scattering, by introducing dependence on electric field magnitude, doping density, and lattice temperature [7–11]. Some mobility models also describe MOS surface conduction. This is done by a dependence on components of the electric field relative to current direction and surface orientation, dependence on position within the device to describe surface scattering, and dependence on carrier density to account for screening effects [12-15]. The physical appropriateness of such models has also been discussed [16].

Techniques for the discretization of the macroscopic equations via finite differences (Scharfetter-Gummel approach [9]) or finite elements, and their subsequent solution using coupled or decoupled techniques, have been



Control volumes for a triangular mesh.

widely discussed in the literature [6, 17, 18]. While physically motivated mobility models have usually been a part of these previous works, issues involved in mobility model evaluation in the discrete environment have usually been glossed over. This lack of completeness has often been attributed to the relatively weak variation in mobility values compared to, say, carrier concentrations or current densities. However, as one goal of device simulation is increasing understanding of internal device behavior, physically motivated mobility models must be properly discretized. Where statements about mobility evaluation have been made [19], mobility evaluation for the continuity equation at (i, j) seems to introduce excessive nodal coupling, namely to  $(i \pm 1, i \pm 1)$ ,  $(i \pm 2, j)$ , and  $(i, j \pm 2)$ , in addition to the usual four nearest nodes to (i, j) (notation as in Fig. 4, shown later). While this coupling can be irrelevant in decoupled solution methods or in approximate Newton's methods which do not differentiate mobility when assembling the Jacobian matrix, a rigorous Jacobian matrix evaluation is essential to correct small-signal ac simulation [20, 21]. Our formulation allows proper accuracy to be attained with less nodal coupling than cited above. Our development of physically motivated mobility models is in the context of a well-known hybrid finite element-finite difference discretization scheme [22-25] and is therefore applicable to arbitrary device shapes and mesh refinements.

In this paper, a discretization method extending the Scharfetter-Gummel finite difference approach is first reviewed in Section 2. Discretization of generalized mobility models possessing quite arbitrary functional forms is introduced. Next, the impact of generalized mobility models on sparsity and convergence rate of the discrete equations is discussed in Section 3. Finally, some computational results from a study of short-channel MOSFETs are presented in Section 4 to illustrate our approach.

### 2. Discretization

This section begins by stating the continuum equations taken as describing semiconductor device behavior. A review of the Scharfetter-Gummel/control volume approach to the discretization of these equations follows. The discrete form of a quite arbitrary mobility model is described next within the context of our chosen discretization scheme. The final subsection presents comments specific to rectangular meshes and describes the straightforward extension of this two-dimensional formulation to three dimensions.

### • Continuum equations

The semiconductor transport equations consist of the Poisson equation

$$\nabla \cdot (\varepsilon \nabla \psi) = -q(p - n + N_{\rm D} - N_{\rm A}), \tag{1}$$

together with the continuity equations for holes and electrons.

$$\nabla \cdot \overrightarrow{J}_{p} = q \left( G_{p} - R_{p} - \frac{\partial p}{\partial t} \right), \tag{2a}$$

$$-\nabla \cdot \overrightarrow{J}_n = q \left( G_n - R_n - \frac{\partial n}{\partial t} \right). \tag{2b}$$

The hole and electron current densities are assumed to be given by the equations

$$\vec{J}_p = -q(\mu_p p \nabla \psi + D_p \nabla p), \tag{3a}$$

$$\vec{J}_n = q(-\mu_n n \nabla \psi + D_n \nabla n). \tag{3b}$$

The Einstein relation between diffusivities and mobilities is assumed to hold:

$$D = \frac{kT}{q} \mu. (4)$$

Notation in this section is standard. The reader is referred to the list of symbols in the Appendix.

• The Scharfetter-Gummel/control volume approach
The above equations are discretized by a hybrid finite
element-finite difference method [22–25] using the
Scharfetter-Gummel approach [9] for computing carrier
current densities. The discretization methods are discussed
in the context of a nonuniform, two-dimensional triangular
mesh.

The discretization of the Poisson equation (1) is independent of the mobility model used, and since

techniques for the discretization of elliptic partial differential equations are widely known, they are not described here. It suffices to note that since the Poisson equation is coupled to the remaining equations, the charge weighting scheme used for the Poisson equation must be identical to the one used for the continuity equations. As long as this identity is satisfied, a finite element approach can be used for the Poisson equation even though finite differences are used to discretize the current continuity equations.

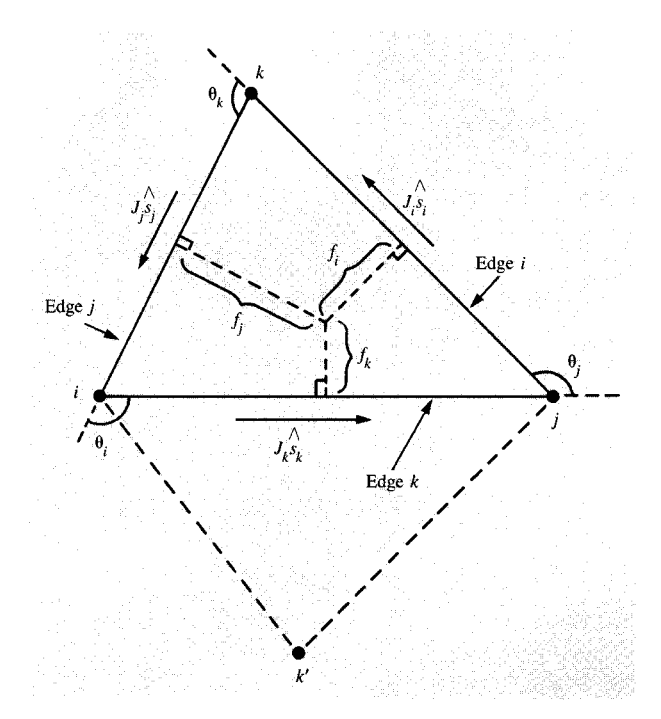
The continuity equations (2) are treated using the method of "control volumes." The discrete form of the divergence operator in the continuity equations is derived by assigning to each node in the mesh a control volume. The volume is bounded by the perpendicular bisectors of all element edges emanating from a given node, as shown in Figure 1. Currents entering or leaving the control volume through the perpendicular bisectors (considered as flux cross sections) are then summed and set equal to the rate of change of carrier density at the node, weighted by the control volume. Summing over all elements e(i) which contain node i, the result is (see Figure 2 for element notation)

$$\sum_{q(i)} (J_k^p f_k - J_j^p f_j) = q v_i \left( G_i^p - R_i^p - \frac{\partial p_i}{\partial t} \right), \tag{5a}$$

$$-\sum_{e(i)} (J_k^n f_k - J_j^n f_j) = q v_i \left( G_i^n - R_i^n - \frac{\partial n_i}{\partial t} \right).$$
 (5b)

Here,  $J_k^p(J_k^n)$  is the hole (electron) current density flowing along the side k in a counterclockwise direction and  $f_k$  is the flux cross section for the side k (similarly for side j).  $v_i$  is the control volume associated with the node i.  $G_i^p$ ,  $R_i^p$ , and  $\partial p_i/\partial t$  are the functions  $G_p$ ,  $R_p$ , and  $\partial p/\partial t$  evaluated at node i (similarly for  $G_i^n$ ,  $R_i^n$ , and  $\partial n_i/\partial t$ ). A time stepping algorithm is used to convert the time derivatives to discrete form; in our case fully implicit time discretization is employed.

Although  $J_k$  may be viewed as the current density flowing from node i to node j ( $J_i$ :  $j \rightarrow k$ ;  $J_i$ :  $k \rightarrow i$ ),  $J_k$  is actually an averaged value of the projection of the current density  $\vec{J}$ onto a unit vector in the direction of the mesh edge  $i \rightarrow j$ , e.g.,  $\vec{J} \cdot \hat{s}_k$ . A discrete form of the transport equations (3) giving the current density  $J_{k}$  was derived originally by Scharfetter and Gummel [9], and extended to two dimensions by Slotboom [26]. By assuming that the components of the electric field  $\vec{E}$  and current density  $\vec{J}$ along an edge are varying sufficiently slowly to be treated as constant along the edge, the current transport equation (3b) can be reduced to a one-dimensional, linear, first-order ordinary differential equation for the carrier density n[similarly (3a) for holes]. This equation can be integrated to yield n along the element edge, and by setting  $n(\vec{x}_a) = n_a$  at the nodes  $[p(\vec{x}_a) = p_a$  for holes], the following equations may be derived for the Scharfetter-Gummel current densities  $J_k$ :



Element notation

$$J_k^p = \frac{q\bar{\mu}_k^p}{\beta L_k} \left[ p_i Z(\Delta_k) - p_j Z(-\Delta_k) \right], \tag{6a*}$$

$$J_k^n = \frac{q\bar{\mu}_k^n}{\theta L_k} \left[ n_j Z(\Delta_k) - n_i Z(-\Delta_k) \right], \tag{6b*}$$

where

$$\Delta_k = \beta(\psi_j - \psi_i), \qquad Z(u) = \frac{u}{e^u - 1},$$

 $\bar{\mu}_k^p(\bar{\mu}_k^n)$  is the average hole (electron) mobility along edge k, which is of length  $L_k$ , and  $\beta$  is the inverse thermal voltage q/kT. [The asterisk in equation numbers here and later indicates that the equation is equally valid with a cyclic permutation of indices of the two-dimensional element; i.e., (i, j, k) can be replaced with (j, k, i) or (k, i, j).]

• Discrete form of generalized mobility models

To incorporate a generalized mobility into the ScharfetterGummel formulation, consider the electron mobility model

$$\mu_n = \mu_n(\vec{E}, \hat{j}, \hat{s}, \vec{x}, N, n, T),$$
 (7)

where  $\vec{E}$  is the electric field,  $\hat{j}$  the unit current density direction vector,  $\hat{s}$  the unit normal to an insulator-semiconductor interface,  $\vec{x}$  is position, and N, n, and T are doping, electron density, and temperature, respectively.

This form is sufficiently general to include dependence on electric field components relative to current direction

 $(\vec{E} \cdot \hat{j}, \vec{E} \times \hat{j})$ , surface orientation  $(\vec{E} \cdot \hat{s}, \vec{E} \times \hat{s})$ , or some hybrid  $[(E \times \hat{j}) \cdot (\hat{s} \times \hat{j}) \text{ (see [13])}]$ . In addition, explicit dependence on position  $\vec{x}$  and the standard dependencies on doping density N, carrier concentration n (or p for hole mobility), and lattice temperature T are included. The approach used is to derive appropriate discrete representations for the average along an element edge of each mobility argument and to then substitute these expressions into the functional form of the mobility. This discrete average mobility along an element edge is then used in the Scharfetter-Gummel current density expressions (6). The overall method is thus independent of the specific form of the mobility model used, as given in (7). To be quite specific, and for simplicity, arguments for the mobility (7) are determined along edge k of an element as shown in Fig. 2. Cyclic permutations of indices generate analogous expressions for mobility arguments along edges i and j.

Mobility arguments in this general case include both scalars and vectors. For scalar quantities, a discrete form can be obtained simply by forming an appropriate average along edge k. For vector quantities, obtaining the needed magnitude and direction is more complex, potentially requiring the use of quantities at adjacent nodes k and k' as well (see Fig. 2). The approach is simplified by calculating the contributions to the current from node combinations (ijk) and (ijk') separately, which permits element-wise assembly of the global matrix of equations. Finally, it is crucial to note that to ensure local and global conservation of charge, we must have  $J_k$  depend on quantities at nodes i and j antisymmetrically; i.e.,  $J_k$  must reverse sign if i and jare interchanged in the formulation of  $J_k$ . The Scharfetter-Gummel current density expressions (6) possess this antisymmetry property for constant mobility; hence, the mobility calculated along edge k must be unaffected if indices i and j are interchanged during argument evaluation.

For scalar quantities, the mobility is evaluated by averaging along edge k. Our precept is to average the physical quantities defined along an element edge exactly as that quantity is defined in functional form in the overall formulation. Accordingly, the total impurity concentration, which in our case varies as a step function between nodes, is averaged as

$$\bar{N}_k = \frac{N_i + N_j}{2}. ag{8*}$$

Carrier densities, in contrast, are assumed in the derivation of the current density expressions (6) to vary exponentially with position, and hence should be averaged accordingly. Directly averaging the exponential form of p and n along edge k yields

$$\bar{p}_k = p_i Q(\Delta_k) + p_i Q(-\Delta_k), \tag{9a*}$$

$$\bar{n}_k = n_j Q(\Delta_k) + n_i Q(-\Delta_k), \tag{9b*}$$

where

292

$$Q(u) = \frac{1}{u} - \frac{1}{e^u - 1}$$
.

Lattice temperature T is usually assumed to be constant throughout the device, in which case no averaging is necessary. For T slowly varying with position, linear interpolation can be used, but more detailed thermal effects which involve hole and electron temperatures imply the use of some energy balance relations, and are therefore beyond the scope of this analysis.

Vector quantities require extraction of both magnitude and direction from values of scalar quantities at the nodes. Explicit dependence on position  $\vec{x}$  is easily treated by using the midpoint of edge k:

$$\vec{x}_{\text{mid}} = \frac{\vec{x}_i + \vec{x}_j}{2}.\tag{10*}$$

A unit vector  $\hat{s}$  is defined as being normal to the semiconductor-insulator interface at the interface point  $\vec{x}_s$  closest to  $\vec{x}_{\text{mid}}$ , as shown in **Figure 3**. The distance from the interface is then

$$d_s = |(\vec{x}_{mid} - \vec{x}_s) \cdot \hat{s}|. \tag{11}$$

Potential varies linearly over the triangular element in this formulation. The components of the electric field along element edges i, j, k are

$$E_i = \vec{E} \cdot \hat{s}_i = -\frac{\psi_k - \psi_j}{L_i},\tag{12a}$$

$$E_j = \vec{E} \cdot \hat{s}_j = -\frac{\psi_i - \psi_k}{L_i},\tag{12b}$$

$$E_k = \vec{E} \cdot \hat{s}_k = -\frac{\psi_j - \psi_i}{L_k}.$$
 (12c)

Only two of these components are independent, since they are related by the expression

$$L_{i}E_{i} + L_{i}E_{i} + L_{k}E_{k} = 0. {13}$$

The electric field  $\vec{E}$  may therefore be reconstructed from any pair of components along the element edges:

$$\vec{E} = \frac{1}{\sigma_i^2} [(E_j - \rho_i E_k) \hat{s}_j + (E_k - \rho_i E_j) \hat{s}_k]$$
 (14a)

$$= \frac{1}{\sigma_i^2} [(E_k - \rho_j E_i) \hat{s}_k + (E_i - \rho_j E_k) \hat{s}_i]$$
 (14b)

$$= \frac{1}{\sigma_k^2} [(E_i - \rho_k E_j) \hat{s}_i + (E_j - \rho_k E_i) \hat{s}_j],$$
 (14c)

where

$$\begin{split} & \rho_j = \hat{s}_k \cdot \hat{s}_i = \cos \theta_j, \, \rho_k = \hat{s}_i \cdot \hat{s}_j = \cos \theta_k, \, \rho_i = \hat{s}_j \cdot \hat{s}_k = \cos \theta_i, \\ & \sigma_j = \hat{s}_k \times \hat{s}_i \cdot \hat{z} = \sin \theta_j, \, \sigma_k = \hat{s}_i \times \hat{s}_j \cdot \hat{z} = \sin \theta_k, \\ & \sigma_i = \hat{s}_i \times \hat{s}_k \cdot \hat{z} = \sin \theta_i. \end{split}$$

The problem of determining a current direction  $\hat{j}$  is made difficult by the fact that the Scharfetter-Gummel current

density expressions (6) lead to an ambiguous definition of the current density  $\vec{J}$  within a triangular element. The Scharfetter-Gummel current densities along the edges are assumed to represent average values of the components of the current density  $\vec{J}$  along the edges:

$$J_i = \vec{J} \cdot \hat{s}_i; \qquad J_j = \vec{J} \cdot \hat{s}_j; \qquad J_k = \vec{J} \cdot \hat{s}_k.$$
 (15)

This suggests that the current density  $\vec{J}$  can be recovered from pairs of components along the edges, as was done for the electric field  $\vec{E}$ . However, the Scharfetter-Gummel current densities as given by (6) are all independent, since

$$L_i J_i + L_i J_i + L_k J_k \neq 0, \tag{16}$$

and therefore the three possible compositions formed from pairs of sides,

$$\vec{J}_{jk} = \frac{1}{\sigma_i^2} \left[ (J_j - \rho_i J_k) \hat{s}_j + (J_k - \rho_i J_j) \hat{s}_k \right], \tag{17a}$$

$$\vec{J}_{ki} = \frac{1}{\sigma_j^2} \left[ (J_k - \rho_j J_i) \hat{s}_k + (J_i - \rho_j J_k) \hat{s}_i \right], \tag{17b}$$

$$\vec{J}_{ij} = \frac{1}{\sigma_k^2} [(J_i - \rho_k J_j)\hat{s}_i + (J_j - \rho_k J_i)\hat{s}_j],$$
 (17c)

are all different. For the purpose of calculating mobility along edge k, a vector current density  $\vec{J}_k$  existing in the vicinity of edge k is required. This is obtained by a weighted average of the two vector compositions which involve edge k:

$$\vec{J}_{k} = \frac{\vec{J}_{ki}f_{i} + f_{j}\vec{J}_{jk}}{f_{i} + f_{j}}.$$
(18\*)

Using flux cross sections to form this average more heavily weights the Scharfetter-Gummel current density composition which includes the shorter of the two edges i and j; current density along a shorter edge is assumed to be known more accurately. By defining the weighting factors

$$w_{ki} = \frac{f_i}{(f_i + f_j)\sigma_j^2},\tag{19a*}$$

$$w_{kj} = \frac{f_j}{(f_i + f_j)\sigma_i^2},\tag{19b*}$$

the current density  $\overrightarrow{J}_k$  may be expressed as

$$\vec{J}_{k} = [w_{ki}(J_{k} - \rho_{j}J_{i}) + w_{kj}(J_{k} - \rho_{i}J_{j})]\hat{s}_{k} + w_{ki}(J_{i} - \rho_{j}J_{k})\hat{s}_{i} + w_{kj}(J_{j} - \rho_{i}J_{k})\hat{s}_{j},$$
(20\*)

and the current direction at edge k is finally given by

$$\hat{J}_k = \vec{J}_k / |\vec{J}_k|. \tag{21*}$$

Since this result is normalized to unity magnitude, an arbitrary constant mobility can be used to initially determine  $J_i$ ,  $J_j$ , and  $J_k$ .

It is important to note that although the mobility is expressed in terms of current and the current depends on

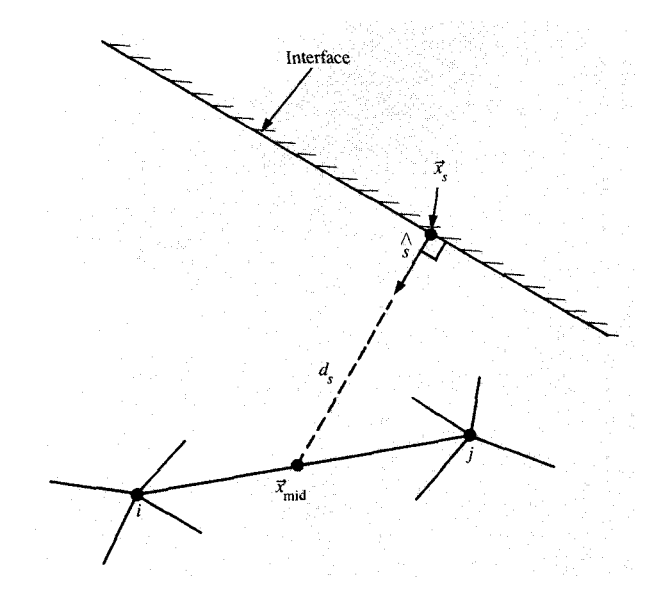


### Figure 3

Determination of distance from semiconductor-insulator interface.

mobility, the expression for current is not implicit. This is because only the current direction affects the mobility, while the mobility in turn affects only the current magnitude (if the Einstein relation holds). In practice, Scharfetter-Gummel current densities along all three edges of a triangular element are first calculated using an arbitrary constant mobility. From these, the current directions, obtained as outlined above, are in turn used to determine the mobility along the element edges. Finally, the original Scharfetter-Gummel current densities are scaled using the values of the mobility calculated.

### • Comments on and extensions of the method

The discretization method described above for triangular meshes can be readily applied to rectangular meshes as well. If a triangular mesh is constructed so that the shortest edges of each triangular element are aligned with the coordinate directions, as shown in Figure 4, then the flux cross sections for each diagonal element edge are zero. As a result, Scharfetter-Gummel currents along the diagonals may be ignored, and the mesh is effectively rectangular in nature. If the Scharfetter-Gummel/control volume approach as described here is applied directly to the formation of continuity equations at (i, j) using the triangular mesh of Fig. 4(a), coupling is to the four nearest neighbor nodes indicated. Using the triangular mesh of Fig. 4(b), the mobility evaluation couples to all eight neighboring nodes indicated. As constructs of type Fig. 4(a) will not cover a rectangular domain, our method produces variable coupling to between four and eight nodes for a triangulation of a

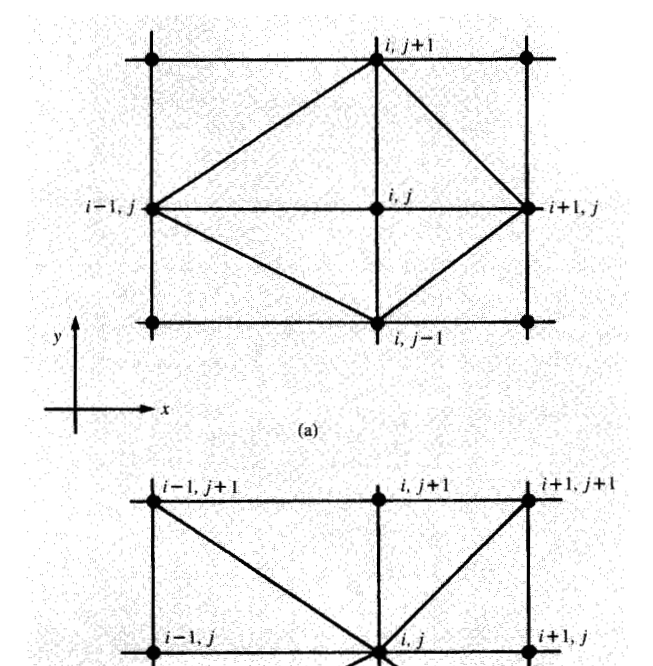


Figure 4

Rectangular mesh and two possible triangulations.

(b)

rectangular mesh. Techniques for discretization on rectangular meshes are not based directly on approaches for triangular meshes, however. Since finite difference meshes do not contain diagonal mesh segments, neither possibility for diagonal orientation may be favored. Since mobility along edge (i + 1/2, j) must be unchanged whether calculated in the context of nodal equation (i, j) or (i + 1, j) [analogously for all four mesh directions emanating from (i, j), nodal equation (i, j) must minimally couple to all eight nearest neighbors, as shown in Fig. 4(b). As cited previously [19], even larger coupling is not precluded. The mobility formulation described generates no more nodal coupling than a finite difference approach; in fact, coupling varies over the rectangular mesh and is often less. This coupling is irrelevant for decoupled methods or for approximate Newton's methods where mobility derivatives are not included in the Jacobian. Small-signal ac analysis, however, does not permit this liberty to be taken.

Although the extension of the above methods to three dimensions is difficult in practice, it is at least straightforward conceptually [23, 25]. Triangular mesh

techniques could be generalized to tetrahedral meshes. Instead, right triangular prism finite elements have been selected. At present, this only permits 3D meshes to be created by replication of a 2D mesh in the z-axis direction. To date these elements have been sufficient for our needs. This element has control volumes bounded by planar perpendicular bisectors, with Scharfetter-Gummel current densities flowing along element edges as before. Electric fields are evaluated rigorously at element edge midpoints consistent with the chosen 3D shape function for the potential:

$$\phi_{3D}(x, y, z) = a_0 + a_1 x + a_2 y$$

$$+ a_3 z + a_4 x z + a_5 y z. \tag{22}$$

Current direction is calculated similarly to the scheme described for current density components in the x-y plane; z-direction current density components are appropriate averages of the three z-directed Scharfetter-Gummel current densities present in the 3D element.

# 3. Implementation and convergence experiments

This section highlights the salient features of the FIELDAY [22–25] simulation program that relate to the mobility modeling of Section 2 and presents selected results of computational experiments aimed at understanding the convergence behavior of the program.

### **§** Implementation

The FIELDAY device simulation program is a two- or threedimensional transient device simulation program based on the Scharfetter-Gummel/control volume approach. For some years, the program has offered both decoupled and coupled solution approaches [27], with the coupled solution method favored for typical device problems. As such, the coupled method is assumed in all that follows. The Newton's method matrix equations are solved by using direct matrix factorization techniques. Implementation of the mobility formulation of Section 2 was quite straightforward in concept. As our program also allows small-signal ac simulation [20], most of the programming involved the differentiation of the mobility formulation with respect to the independent variables  $(\psi, n, p)$  as required for Jacobian formulation in the ac case. However, for non-ac simulation needs, the code skips mobility differentiation by default. This leads to an increase in matrix sparsity but to a decrease in measured asymptotic convergence rate of the program, as will be seen; however, this loss of asymptotic convergence rate rarely penalizes the typical user, who terminates program execution well away from truncation.

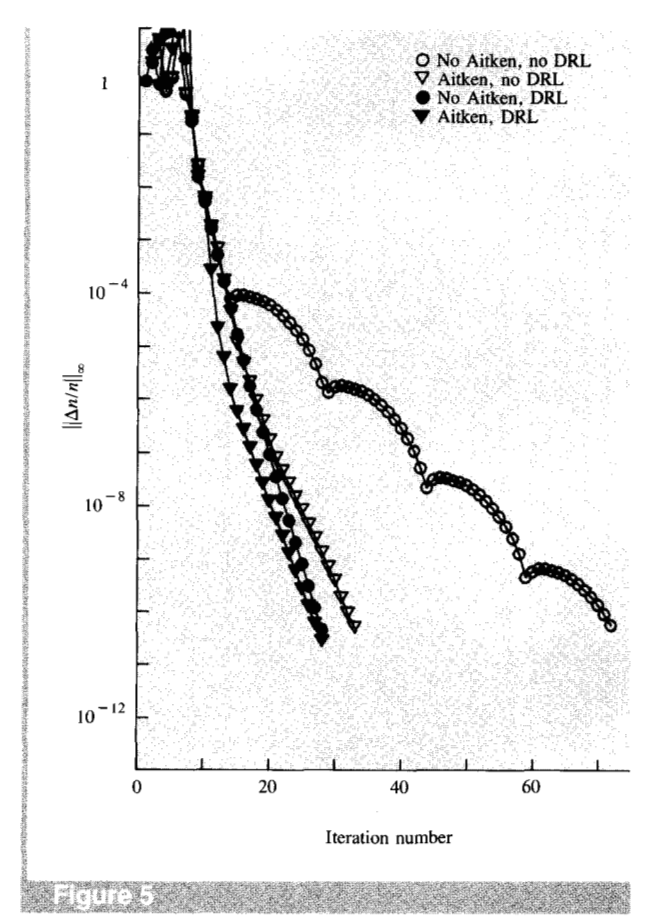
The overall goal in implementation was to isolate as much as possible the functional form of the mobility model from the details of model evaluation and global matrix assembly. This has been accomplished by localizing the mobility model

into a single FORTRAN function. For ac simulation this function must also return partial derivatives of the mobility with respect to all function arguments. All other aspects of problem discretization are separate and removed from this function, making the introduction of alternate or exploratory mobility models simple for the typical program user.

The program currently contains eight different mobility models selected from the literature [7–9, 12–14, 16, 28], as well as two mobility models [15, 29] developed in-house. Temperature dependence of the models was implemented either as specified by the original reference or by utilizing general expressions of temperature dependence of mobility [10, 11]. A multiplicity of mobility models were implemented primarily to allow direct comparisons between published mobility models to be made easily and equitably.

### • Convergence experiments

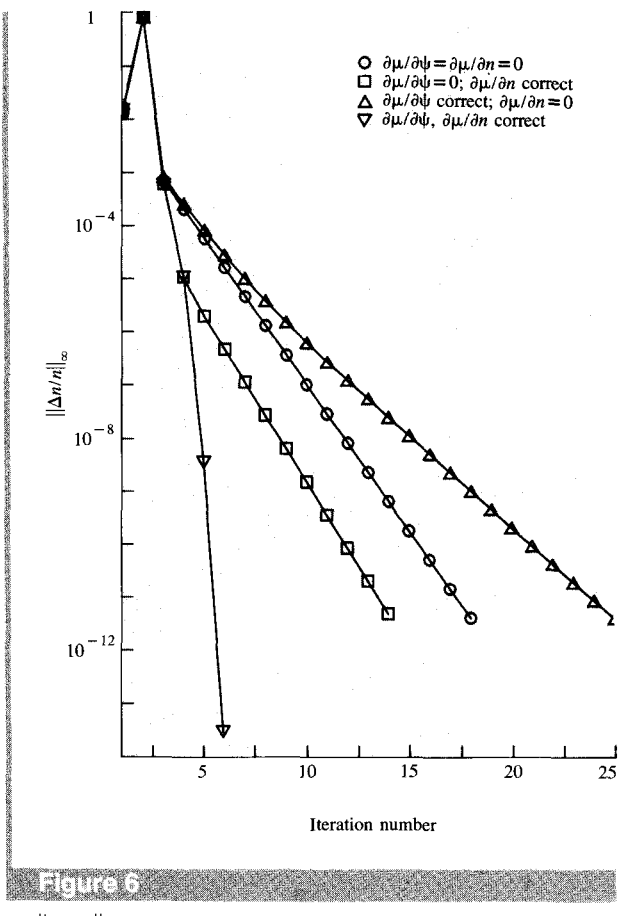
In the early phases of program development, a severely degraded asymptotic convergence rate was observed whenever a mobility function was evaluated with  $E_{\parallel} =$  $\max(E \cdot \hat{j}, 0)$ . Use of this particular argument is quite pervasive in mobility modeling, as it yields the component of E in the direction of carrier current flow. Initially, Aitken extrapolation [30] was invoked with dramatic improvement in convergence rate; however, the real cause of our poor convergence performance was traced to the argument itself. Unfortunately, in regions of minute current flow (in our case, electron current in an n-MOSFET well below the Si-SiO<sub>2</sub> interface), where carrier concentrations much less than the intrinsic carrier concentration are found, current information is quite noisy. As a result, this vector dot product is quite noisy, causing the local carrier quasi-Fermi solution to become perturbed in response to small mobility changes. Because our program convergence for carriers is based on monitoring  $\|\Delta n/n\|_{\infty}$  or  $\|\Delta p/p\|_{\infty}$ , which asymptotically measures convergence of quasi-Fermi levels (assuming converged potential), a net loss in convergence rate was observed. This problem was quite easily rectified by implementing a dynamic range limitation (DRL) feature in the evaluation of this argument as follows. The program calculates the maximum current density  $J_{\text{max}}$  present in the device domain; for any current densities below a value  $\gamma J_{\rm max}$  $(\gamma \sim 10^{-12})$  for our 16.8 decimal digit arithmetic), this problematic argument is set to zero prior to mobility evaluation. DRL has never been observed to alter device solutions in any meaningful way; however, roughly the same dramatic improvement in convergence rate was obtained as for Aitken extrapolation. Figure 5 depicts this initially poor convergence rate for an n-MOSFET using mobility after Reference 14, as well as the two improvements (Aitken and DRL) described. The same rather crude initial guess was used in all cases. A final curve using both Aitken and DRL shows little net improvement over either of the two approaches individually. Note that the companion plot of



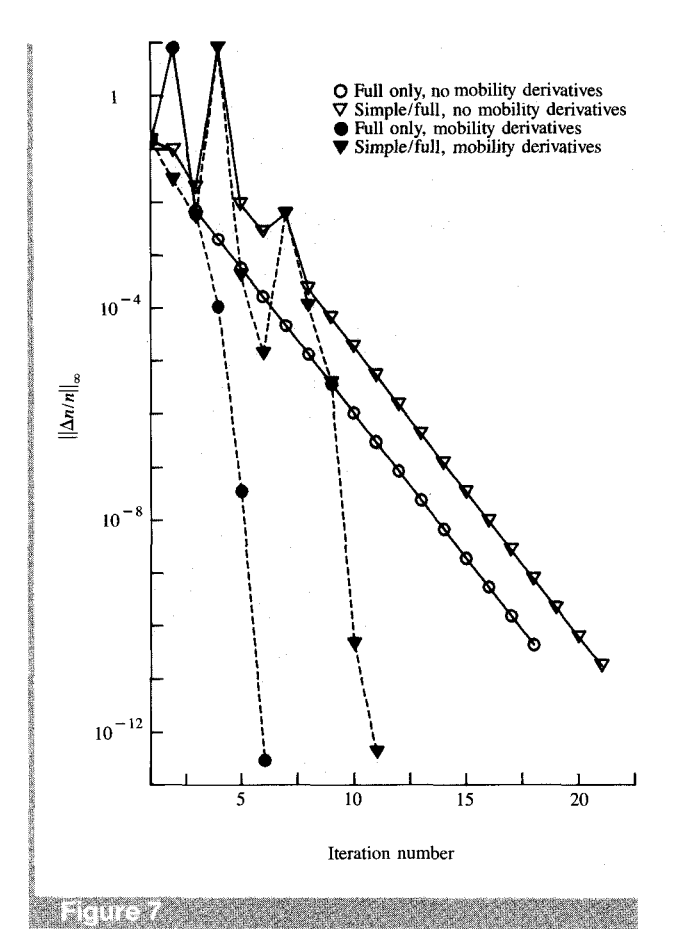
 $\|\Delta n/n\|_{\infty}$  versus iteration number with and without Aitken extrapolation and DRL.

 $\|\Delta\psi\|_{\infty}$  versus iteration number (not shown) does not show this behavior but rather reaches truncation ( $\sim 10^{-12}$ ) in less than 20 iterations for all four curves.

Examination of each curve in Fig. 5 shows a predictable lack of quadratic convergence. Although Newton's method is being practiced here, the Jacobian matrix is assembled neglecting derivatives of mobility with respect to independent variables  $(\psi, n, p)$ . Figure 6 clarifies this situation for the same n-MOSFET and mobility model using a somewhat improved initial guess for the solution. Four curves showing the various combinations of proper  $\partial \mu / \partial \psi$ and  $\partial \mu / \partial n$  evaluation (hole continuity equation not solved in this example) are presented. Linear convergence is observed for all combinations where the Jacobian is based on nonrigorous mobility differentiation, with correct differentiation with respect to n seemingly more important than differentiation with respect to  $\psi$ . Quadratic convergence is clearly demonstrated when proper Jacobian formation is practiced. The companion plot of potential convergence versus iteration number (not shown) shows qualitatively similar results, except that convergence here is roughly 2-3



 $\|\Delta n/n\|_{\infty}$  versus iteration number with and without inclusion of  $\partial \mu/\partial \psi$  and  $\partial \mu/\partial n$  in the Jacobian.



 $\|\Delta n/n\|_{\infty}$  versus iteration number with and without proper mobility differentiation and modified Newton's method.

iterations faster, and the case of  $\partial \mu/\partial n = \partial \mu/\partial \psi = 0$  converged second fastest of the four combinations.

One final convergence experiment merits discussion. In our case, as is often done, Jacobian assembly/matrix factorization steps are not performed at every Newton's step. but rather the previously factored Jacobian is used for n steps (here n = 2 was appropriate [31]) before a new Jacobian is calculated. The attendant savings in matrix assembly/factorization are traded against a potentially slowed convergence path. Figure 7 quantifies this expectation. Quadratic convergence is observed for both cases where mobility differentiation was included in the Jacobian, but convergence was slowed by using the algorithm of executing two "simple" Newton's steps to every "full" step. This same conclusion holds in the case of linear convergence resulting when mobility differentiation was neglected in Jacobian formation. Qualitatively similar results are seen in the companion potential convergence plot (not shown).

Convergence results similar to those described have been qualitatively observed with all the mobility models

implemented to date in the program. Some models take somewhat longer to converge to the same accuracy tolerance when started from the same initial guess, but the differences are not appreciable. Table 1 shows the number of iterations and the CPU times required (on an IBM 3081) for convergence of an n-MOSFET-biased  $V_G = 1.4 \text{ V}$ ,  $V_D = 3 \text{ V}$ , and  $V_{\rm R} = -0.75$  V starting with a crude initial guess. To expedite mobility model identification, the following mnemonics are used to refer to the given references: VS [7], CT [8], SG [9], TB [16], CTY [29], SGY [12], TBY [14], FO [28], BW [15], and SS [13]. In addition, CONS denotes use of a constant mobility. From Table 1, the fastest convergence was for CONS in 31 iterations; the slowest for VS in 57 iterations. Most physically interesting models require about 45 iterations; hence, little penalty is paid for switching between these various mobility models.

# 4. Computational results for short-channel MOSFETs

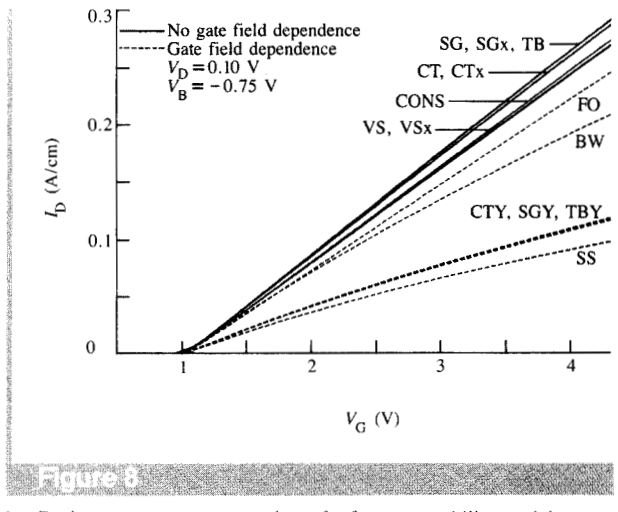
Two examples of computational results from a study of short-channel MOSFETs are discussed in order to illustrate

the mobility modeling approach of Section 2. The model n-MOSFET to be discussed has the following salient features: metallurgical channel length  $L_{\rm met}=1.1~\mu{\rm m}$ , source- and drain-substrate junctions modeled as step junctions with  $N_{\rm D(source)}=N_{\rm D(drain)}=2\times10^{20}~{\rm cm}^{-3}$  and  $N_{\rm A(sub)}=3.3\times10^{15}~{\rm cm}^{-3}$ , single acceptor-type threshold adjust implant to yield threshold voltage  $V_{\rm T}\sim1$  V assuming n<sup>+</sup> polysilicon gate and  $t_{\rm ox}=22.5~{\rm nm},~T=300~{\rm K}.$  The computational mesh contains 962 nodes and 1822 elements.

### • Transfer characteristics

The transfer characteristic ( $I_D$  versus  $V_G$ ) at low  $V_D$  is one of the first measurements performed during routine laboratory characterization of MOSFETs. This plot is an excellent indicator of inversion layer mobility and device threshold voltage. As such, this plot illustrates the differences between the various mobility models implemented in FIELDAY. Figure 8 shows such a plot for the same MOSFET differing only by the mobility model selected for the computation. In addition to the eleven mobility models listed in Table 1, three additional curves are shown in Fig. 8, designated by VSx, CTx, and SGx. These mobility models are exactly the VS, CT, and SG models, respectively, with one important difference: A different electric field strength argument is used to evaluate the mobility function. The eleven mobility models in Table 1 have quite distinctive dependencies but do depend on one argument in common:  $E_{\parallel} = \max(E \cdot \hat{j}, 0)$ as previously introduced. One possible alternative to  $E_{\parallel}$ , which was previously seen to cause some convergence problems and is complex to calculate, is as follows. Instead of forming the vector dot product between electric field and current flow direction at each element edge as for  $E_{\parallel}$ , numerical current flow is in some sense constrained to lie along element edges. Thus, in an ad hoc fashion, one might hypothesize that the electric field in the current flow direction is approximated by  $E_{\text{side}}$ , the magnitude of the electric field along an element side.  $E_{\text{side}}$  is seen to be the absolute value of the right-hand sides of Eqs. (12a-c). As an added bonus to easy computation, use of  $E_{\text{side}}$  does speed up convergence somewhat, typically requiring 20 percent fewer Newton's iterations than the use of  $E_{\parallel}$  to evaluate the same mobility function. Unfortunately, this argument is admittedly nonphysical, retaining an undesirable dependence on mesh orientation. It is the use of this argument,  $E_{\text{side}}$ , with mobility functions VS, CT, and SG, that is designated VSx, CTx, and SGx in Fig. 8.

The fourteen curves of Fig. 8 naturally fall into two groups: those with no dependence on gate electric field (solid lines) and those with explicit dependence on gate field (dotted lines). Obviously, models without gate field dependence are inappropriate for MOSFET modeling but may be the models of choice in bipolar transistor modeling. The relatively small differences between the solid curves are due to the low field mobility values for electrons at the



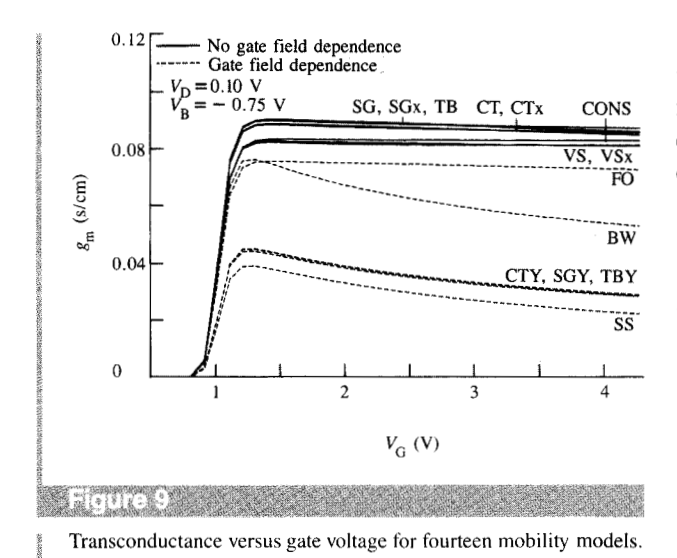
Drain current versus gate voltage for fourteen mobility models.

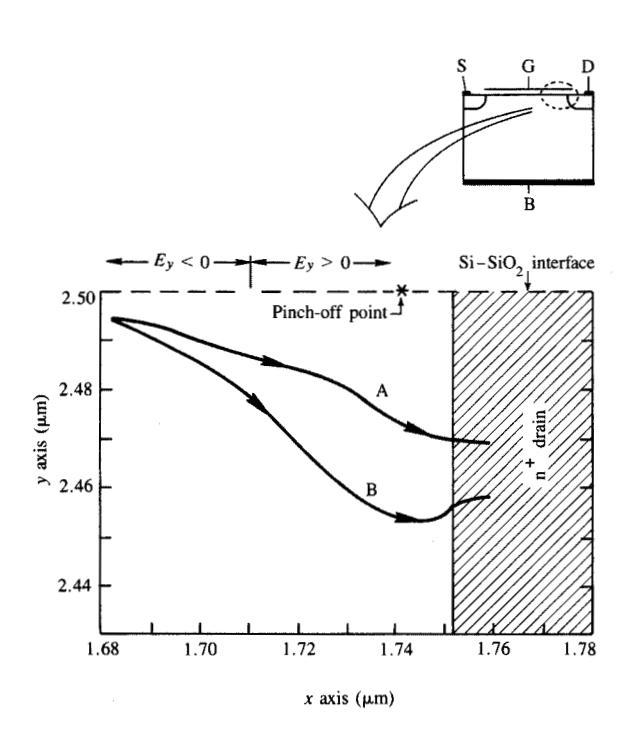
**Table 1** Iterations and CPU time required for eleven mobility models.

Mnemonic	Iterations	CPU time (s)
CONS	31	148
VS	57	284
CT	46	257
SG	46	242
TB	46	241
CTY	47	288
SGY	46	235
TBY	40	212
FO	46	245
$\mathbf{BW}$	46	273
SS	44	242

interface as given by each model. These low field mobility values are (1) SG, SGx, TB: 659 cm<sup>2</sup>/V-s; (2) CT, CTx: 646 cm<sup>2</sup>/V-s; (3) CONS, VS, VSx: 600 cm<sup>2</sup>/V-s. The ordering of the curves agrees precisely with the order of these low field mobility values. Note that the models using  $E_{\rm side}$  (x suffix) are remarkably close to their  $E_{\parallel}$  counterparts.

The six remaining mobility models are all explicitly influenced by the increase in gate field for increasing  $V_{\rm G}$ . This results in a transconductance degradation as  $V_{\rm G}$  increases and is reflected by the slow decrease in  $g_{\rm m}=\partial I_{\rm D}/\partial V_{\rm G}$  as  $V_{\rm G}$  increases in Fig. 8. Transconductance versus  $V_{\rm G}$  is shown explicitly in Figure 9 for all mobility models under the bias conditions of Fig. 8. Note that the various mobility models show significant differences in predicted current flow and transconductance; in all cases parametric values for each model are as provided in the cited references. Each model is supposedly a good fit to experimental data; since the models disagree among themselves, a large spread





Average electron flux path in the pinch-off region of an n-MOSFET. Curve A is the result for any of the eleven mobility models of Table 1;

in the hardware which calibrated each model is implied. The obvious conclusion is that a MOSFET mobility model must be calibrated to a given fabrication process and potentially recalibrated for each new technology generation.

Data of the type shown in Fig. 8 are nearly universally used to extract device threshold voltage. This is done by finding the  $V_{\rm G}$  axis intercept of a line drawn tangent to the device characteristic at its point of inflection (typically occurring for  $V_{\rm G} \sim 0.5$  to 1 V above threshold). The  $V_{\rm G}$  intercept found is then equated to  $V_{\rm T} + 0.5~V_{\rm D}$ . Results of such a  $V_{\rm T}$  extraction for the fourteen curves of Fig. 8 are given in Table 2. The  $V_{\rm T}$  values listed are very tightly grouped, having an average value of 0.98689 V with a standard deviation of 0.00408 V. Virtual independence of  $V_{\rm T}$  from mobility is an anticipated result, as alternate definitions of  $V_{\rm T}$  based on a fixed degree of band bending [32] or on an integral of inversion charge [33] do not depend on mobility at all. For extraction of  $V_{\rm T}$  as was done here, the mobility model selected is extremely noncritical.

### Pinch-off

The preceding subsection might leave the impression that selected simulations might be performed using  $E_{\text{side}}$  instead of  $E_{\parallel}$  to evaluate mobility. While this is true in some cases, it is certainly not universally appropriate, as will now be seen. The occurrence of pinch-off in an n-MOSFET biased such that  $V_G \lesssim V_D + V_T$  is a well-known effect. It is at this point, at the drain end of the channel, that electrons are forced to dip away from the Si-SiO2 interface on their course from source to drain. Electron current here consists of both drift and diffusion components. Additionally, high electric fields and a highly two-dimensional field pattern have made this vicinity in the MOSFET cross section one of great interest. Biases of  $V_G = 2.4 \text{ V}$ ,  $V_D = 2 \text{ V}$ , and  $V_B = -0.75 \text{ V}$ have been simulated for the fourteen mobility forms discussed previously. Plots of the average electron flux path in the vicinity of the pinch-off point have been examined and the results fall very convincingly into two categories. (Average electron flux path denotes the flux path above and below which 50 percent of the electron current flows.) The flux path of Figure 10 curve A represents the result obtained by using any of the eleven mobility models of Table 1, i.e., all models except those using  $E_{\text{side}}$  as an argument. Figure 10 curve B shows the flux path obtained using any of the three mobility models having  $E_{\text{side}}$  as an argument. Three important features of the problem are also shown in this figure: (1) the point where the y-directed interface electric field reverses sign from negative (smaller x) to positive (larger x); (2) the point of minimum electron density at the Si-SiO<sub>2</sub> interface denoted by \* (the pinch-off point); and (3) the location of the drain. As electrons pass the  $E_{\nu}$  inflection point while moving from source to drain, they veer into the negative y direction. The interface electron concentration drops markedly, reaching a minimum prior to increasing to meet the highly doped drain (point \*). Once into the highly doped drain, electrons assume a path of minimum resistance until collected at the (distant) drain contact. Most noteworthy in comparing curves A and B is the extent of this

curve B is for mobility evaluated using  $E_{\text{side}}$ 

**Table 2** Threshold voltage extracted for fourteen mobility models.

Mnemonic	$V_{T}$ (V)
CONS	0.99130
VSx	0.98923
VS	0.98968
CTx	0.98940
CT	0.98979
SGx	0.98935
SG	0.98977
TB	0.98970
CTY	0.98162
SGY	0.98165
TBY	0.98159
FO	0.98996
BW	0.98191
SS	0.98145

dip below and around the pinch-off point. Correct behavior is given by curve A; curve B exaggerates this dip for the following reason. The mesh in this region is rectangular in nature, running parallel to the axis directions. For curve B, current flow in the y-direction uses mobility based upon field in the y-direction, which is much less than the field in the primary current flow direction, i.e., the x-direction in this vicinity. Accordingly, vertical currents are somewhat exaggerated, as vertical mobilities at very nearly zero field values are at least ten times larger than their horizontal counterparts. Possessing enhanced vertical mobility, electrons are self-evidently deflected deeper below the interface in response to a very similar field strength.

In summary, although  $E_{\rm side}$  is convenient, it is inappropriate upon examination of internal device solutions. Although somewhat overstated, a similar conclusion applies to any mobility modeling not striving to accurately discretize physically motivated quantities in the evaluation of proper mobility functional forms.

### Summary

Semiconductor modeling based on the Scharfetter-Gummel/control volume approach with generalized mobility models has been presented. This scheme generates no more, and often less, nodal coupling than finite difference formulations on a rectangular mesh and supports the added flexibility of local mesh refinement and arbitrary domain shapes without reprogramming. Extensions of the technique to three-dimensional device simulation are straightforward.

Expectations concerning the convergence rate of the program have been borne out under various assumptions concerning rigor and frequency of Jacobian assembly. Second-order convergence was only observed when mobility derivatives were included in the Jacobian matrix; otherwise, only linear convergence was seen. A degraded convergence rate was also observed and rectified, having been diagnosed as relating to the manner in which mobility was evaluated.

Selected computational results from a study of short-channel MOSFETs illustrated the mobility modeling approach introduced. Eleven different mobility functions were exercised on an otherwise identical n-MOSFET; although absolute drain currents and transconductances predicted were in disagreement, extracted threshold voltages were very similar, as expected. A simplification to mobility evaluation approximating electric field in the direction of current flow was suggested; however, unfavorable results were obtained when internal distributions of carrier flux near pinch-off were examined. Although artificially exacerbated, this result demonstrates the appropriateness of striving for maximum accuracy in mobility modeling through proper discretization of physically motivated arguments.

### **Acknowledgments**

It is a pleasure to acknowledge the following individuals, each of whom has left an indelible influence on the present state of the FIELDAY program: E. M. Buturla, P. E. Cottrell, B. M. Grossman, H. Lustig, C. T. McMullen, and K. A. Salsburg. Special thanks go to B. M. Grossman, E. M. Buturla, and P. E. Cottrell for critical reading of this manuscript and also to M. R. Wordeman, G. Baccarani, R. H. Dennard, and F. H. Gaensslen.

# **Appendix: List of symbols**

Symbol	Definition
$d_s$	Distance from insulator-semiconductor interface
$d_s$ $D_p$ , $D_n$ $E$	Hole, electron diffusivities
$\vec{E}$	Electric field
$E_{i(j,k)}$	Electric field components along edges $i(j, k)$
$E_{\parallel}$	$\max(E \cdot \hat{j}, 0)$
$f_{i(j,k)}$	Flux cross sections of triangular element for
	edges $i(j, k)$
$G_p, G_n$	Hole, electron generation rates
i, j, k	Indices of a triangular element: counterclockwise orientation
ĵ	Unit current direction vector
$\hat{J}_{i(j,k)}$	Unit current direction vector extant for element
<b>→</b>	edge i (j, k)
$\vec{J}_p, \vec{J}_n$	Current density vector
	Hole, electron current density vectors
$J_{i(j,k)}$	Scharfetter-Gummel current densities along element edges $i$ ( $j$ , $k$ )
$\vec{J}_{i(j,k)}$	Total current density vector extant for element
	edge $i(j, k)$
$\overrightarrow{J}_{pq}$	Composition of Scharfetter-Gummel current
	densities of edges $p$ and $q$
k	Boltzmann constant
$L_{i(j,k)}$	Lengths of element edges $i(j, k)$
N	$N_{\rm A} + N_{\rm D}$ , total impurity concentration
$\bar{N}_{i(j,k)}$	Average $N$ on element edge $i(j, k)$

$N_{\rm D}, N_{\rm A}$	Donor, acceptor impurity concentrations
p, n	Hole, electron concentrations
$p_{i(i,k)}, n_{i(i,k)}$	$p(\vec{x}_{i(j,k)}), n(\vec{x}_{i(j,k)})$
$\bar{p}_{i(j,k)},  \bar{n}_{i(j,k)}$	Average hole, electron concentrations along
	element edge $i(j, k)$
q	Electron charge
$Q(\cdot)$	Carrier averaging function
$R_p, R_n$	Hole, electron recombination rates
ŝ	Unit vector normal to insulator-semiconductor
	interface
$\hat{S}_{i(j,k)}$	Unit vectors along element edges $i(j, k)$
	(counterclockwise directed)
t	Time
$T_{\text{ox}}$	Oxide thickness for MOSFET
T	Lattice temperature
$v_{i(j,k)}$	Control volumes associated with vertices $i(j, k)$
$V_{\rm G}, V_{\rm D}, V_{\rm B}$	Gate, drain, substrate applied voltages for
	MOSFET (Source at 0 V)
$V_{T}$	MOSFET threshold voltage
$ \begin{array}{c}                                     $	Weighting factors for current superpositions
$\stackrel{X}{\rightarrow}$	Position vector
$X_{i(j,k)}$	Position vector for node $i(j, k)$
$\vec{x}_s$	Point on insulator-semiconductor interface
	closest to a position $\vec{x}_{mid}$
<del>2</del>	Unit vector in z coordinate direction
$Z(\cdot)$	Bernoulli function
β	q/kT, inverse thermal voltage
$\Delta_{i(j,k)}$	Normalized potential difference $\psi_k - \psi_i (\psi_i - \psi_k)$
70**7	$(\psi_i - \psi_i)$
$\Delta \psi$ , $\Delta n$ , $\Delta p$	Potential, electron, hole update in Newton's
	method
ε	Dielectric permittivity
$\theta_{i(j,k)}$	Angle between $\hat{s}_i$ , $\hat{s}_k$ ( $\hat{s}_k$ , $\hat{s}_i$ ; $\hat{s}_i$ , $\hat{s}_j$ )

k)

Hole, electron mobilities  $\mu_p, \mu_n$ 

Average mobility on element edge i(j, k) $\bar{\mu}_{i(j,k)}$ 

Dot products of unit element edge vectors  $\rho_{i(j,k)}$ 

Cross products of unit element edge vectors  $\sigma_{i(j,k)}$ 

V Electrostatic potential

Maximum norm of function  $\xi$ , i.e., max ( $|\xi|$ ) **||ξ||**<sub>∞</sub>

# References and notes

- 1. Robert A. Warriner, "Computer Simulation of Gallium Arsenide Field-Effect Transistors Using Monte-Carlo Methods," Solid-State & Electron Devices 1, No. 4, 105-110 (July 1977).
- 2. C. Monglestue, "A Monte-Carlo Particle Model and Its Application to a Study of the Influence of the Doping Profiles on the Characteristics of Field-Effect Transistors," Compel 1, No. 1, 7-36 (1982).
- 3. Akira Yoshii, Masaaki Tomizawa, and Kiyoyuki Yokoyama, "Accurate Modeling for Submicrometer-Gate Si and GaAs MESFET's Using Two-Dimensional Particle Simulation," IEEE Trans. Electron Devices ED-30, No. 10, 1376-1380 (October
- 4. R. K. Cook and Jeffery Frey, "An Efficient Technique for Two-Dimensional Simulation of Velocity Overshoot Effects in Si and GaAs Devices," Compel 1, No. 2, 65-87 (1982).
- Walter R. Curtice and Yong-Hoon Yun, "A Temperature Model for the GaAs MESFET," IEEE Trans. Electron Devices ED-28, No. 8, 954-962 (August 1981).

- 6. Siegfried Selberherr, Analysis and Simulation of Semiconductor Devices, Springer-Verlag New York, 1984.
- 7. E. J. Ryder, "Mobility of Holes and Electrons in High Electric Fields," Phys. Rev. 90, No. 5, 766-769 (June 1, 1953).
- 8. D. M. Caughey and R. E. Thomas, "Carrier Mobilities in Silicon Empirically Related to Doping and Field," Proc. IEEE 55, No. 12, 2192-2193 (December 1967).
- 9. D. L. Scharfetter and H. K. Gummel, "Large-Signal Analysis of a Silicon Read Diode Oscillator," IEEE Trans. Electron Devices ED-16, No. 1, 64-77 (January 1969).
- 10. C. Canali, G. Majni, R. Minder, and G. Ottaviani, "Electron and Hole Drift Velocity Measurements in Silicon and Their Empirical Relation to Electric Field and Temperature," IEEE Trans. Electron Devices ED-22, No. 11, 1045-1047 (November
- 11. C. Jacoboni, C. Canali, G. Ottaviani, and A. Alberigi Quaranta, "A Review of Some Charge Transport Properties of Silicon," Solid-State Electron. 20, 77-89 (1977).
- 12. Ken Yamaguchi, "Field-Dependent Mobility Model for Two-Dimensional Numerical Analysis of MOSFET's," IEEE Trans. Electron Devices ED-26, No. 7, 1068-1074 (July 1979).
- 13. S. Selberherr, "Zweidimensionale Modellierung von MOS-Transistoren," Dipl.-Ing. Thesis, Technische Universität Wien, Jänner, 1981.
- 14. Ken Yamaguchi, "A Mobility Model for Carriers in the MOS Inversion Layer," *IEEE Trans. Electron Devices* **ED-30**, No. 6, 658-663 (June 1983).
- 15. Giorgio Baccarani and Matthew R. Wordeman, 'Transconductance Degradation in Thin-Oxide MOSFET's." IEEE Trans. Electron Devices ED-30, No. 10, 1295-1304 (October 1983).
- 16. K. K. Thornber, "Relation of Drift Velocity to Low-Field Mobility and High-Field Saturation Velocity," J. Appl. Phys. 51, No. 4, 2127–2136 (April 1980).
- 17. For a glimpse at current work in the field, see IEEE Trans. Electron Devices, Joint Special Issue on Numerical Simulation of VLSI Devices, Vol. ED-30, No. 9, September 1983, or Proceedings, Third International Conference on the Numerical Analysis of Semiconductor Devices and Integrated Circuits (NASECODE III), Boole Press Limited, Dublin, Ireland, 1983.
- 18. M. S. Mock, Analysis of Mathematical Models of Semiconductor Devices, Boole Press Limited, Dublin, 1983.
- 19. Randolph E. Bank, Donald J. Rose, and Wolfgang Fichtner, "Numerical Methods for Semiconductor Device Simulation." IEEE Trans. Electron Devices ED-30, No. 9, 1031-1041 (September 1983).
- 20. Steven E. Laux, "Calculation of Quasi-Static Device Behavior with Small Computational Burden," Proceedings, Third International Conference on the Numerical Analysis of Semiconductor Devices and Integrated Circuits (NASECODE III), Boole Press Limited, Dublin, Ireland, 1983, pp. 161-166.
- 21. J. L. D'Arcy, G. T. Pearman, E. J. Prendergast, and P. Lloyd, "Physical Simulation of Bipolar Device Structures," Proceedings, Conference on Advanced Research in VLSI, Paul Penfield, Jr., Ed., Cambridge, MA, January 25-27, 1982, pp. 188-200.
- 22. P. E. Cottrell and E. M. Buturla, "Two-Dimensional Static and Transient Simulation of Mobile Carrier Transport in a Semiconductor," Proceedings, First International Conference on the Numerical Analysis of Semiconductor Devices (NASECODE I), Boole Press Limited, Dublin, Ireland, 1979, pp. 31-64.
- 23. E. M. Buturla, P. E. Cottrell, B. M. Grossman, C. T. McMullen, and K. A. Salsburg, "Three-Dimensional Transient Finite Element Analysis of the Semiconductor Transport Equations," Proceedings, Second International Conference on the Numerical Analysis of Semiconductor Devices and Integrated Circuits (NASECODE II), Boole Press Limited, Dublin, Ireland, 1981, pp. 160-165.
- 24. E. M. Buturla, P. E. Cottrell, B. M. Grossman, and K. A. Salsburg, "Finite-Element Analysis of Semiconductor Devices: The FIELDAY Program," IBM J. Res. Develop. 25, No. 4, 218-231 (July 1981).
- 25. B. M. Grossman, E. M. Buturla, and P. E. Cottrell, "Finite-Element Solution of the Semiconductor Transport Equations,"

- Computing Methods in Applied Science and Engineering, VI, J. L. Lyons and R. Glowinski, Eds., North-Holland Press, 1983.
- Jan W. Slotboom, "Computer-Aided Two-Dimensional Analysis of Bipolar Transistors," *IEEE Trans. Electron Devices* ED-20, No. 8, 669-679 (August 1973).
- E. M. Buturla and P. E. Cottrell, "Simulation of Semiconductor Transport Equations Using Coupled and Decoupled Solution Techniques," *Solid-State Electron.* 23, No. 4, 331–334 (April 1980).
- Masao Fukuma and Yuji Okuto, "Analysis of Short-Channel MOSFET's with Field-Dependent Carrier Drift Mobility," *IEEE Trans. Electron Devices* ED-27, No. 11, 2109–2114 (November 1980).
- Mobility is calculated following Reference [16] with the exception of the use of the bulk mobility model of Reference [8] instead of Reference [9].
- Germund Dahlquist and Åke Björck, Numerical Methods, Prentice-Hall, Inc., Englewood Cliffs, NJ, 1974.
- J. M. Ortega and W. C. Rheinholdt, Iterative Solution of Nonlinear Equations in Several Variables, Academic Press, Inc., New York, 1970.
- S. M. Sze, Physics of Semiconductor Devices, 2nd Ed., John Wiley & Sons, Inc., New York, 1981.
- F. H. Gaensslen and R. C. Jaeger, "Temperature Dependent Threshold Behaviour of Depletion Mode MOSFETs: Characterization and Simulations," *Solid-State Electron.* 22, No. 4, 423–430 (April 1979).

Received June 30, 1984; revised November 5, 1984

Robert G. Byrnes Cornell University, School of Electrical Engineering, Ithaca, New York 14853. Mr. Byrnes has been engaged in graduate studies at Cornell University since 1983, pursuing the Ph.D. degree in electrical engineering. His current research interests include semiconductor device, circuit, and process simulation and modeling, especially pertaining to quantized electronic transport processes. He received B.S. and M.S. degrees in electrical engineering from Case Western Reserve University, Cleveland, Ohio, where as a National Science Foundation Fellow in 1983 he was involved in finite element modeling of submicron-geometry charge-coupled devices. During the summer of 1983, he was employed at the IBM Thomas J. Watson Research Center, Yorktown Heights, New York. Mr. Byrnes is a member of the American Physical Society, Eta Kappa Nu, the Institute of Electrical and Electronics Engineers, and Tau Beta Pi.

Steven E. Laux IBM Research Division, P.O. Box 218, Yorktown Heights, New York 10598. Dr. Laux received the B.S. in electrical engineering from Purdue University, West Lafayette, Indiana, in 1976 and the M.S.E. and Ph.D. degrees in electrical engineering from the University of Michigan, Ann Arbor, in 1977 and 1981. Since graduation, he has been employed at the IBM Thomas J. Watson Research Center in Yorktown Heights in the silicon devices and technology area. His interests include MOS device modeling, applied mathematics, and device physics and technology. Dr. Laux is a member of the Institute of Electrical and Electronics Engineers.